J Appl Electrochem (2010) 40:365–374
DOI 10.1007/s10800-009-0005-1

ORIGINAL PAPER

Plasma electrolytic ceramic-like aluminum oxide coatings on iron

S. A. Karpushenkov · G. L. Shchukin · A. L. Belanovich · V. P. Savenko · A. I. Kulak

Received: 4 March 2009 / Accepted: 20 August 2009 / Published online: 30 August 2009

Abstract The process characteristics of plasma-assisted electrochemical treatment of iron in aluminate electrolyte consisted of aqueous 0.1 M $NaAlO_2$ + 0.05 M NaOH have been studied. It has been shown that in the range of DC voltages from 260 to 340 V, it is possible to deposit dense ceramic-like coatings with the thickness increased from 0.3–0.5 μm after 1 min deposition time to 25–30 μm for 1 h of deposition. The coatings were examined by X-ray diffractometry, Fourier-transformed infrared, X-ray photoelectron spectroscopy, scanning electron microscopy, and an electrochemical potentiodynamic voltammetry. It is shown that in pre-spark conditions (100–200 V) and on the initial stages of micro-arc anodizing the forming films contain, along with amorphous aluminum oxide/hydroxide, a substantial amount of iron oxide/hydroxide. The coatings obtained by micro-arc anodizing at 260–360 V for 10–60 min represent amorphous aluminum oxide with inclusions of crystalline corundum phase. The films with a thickness of 4–15 μm deposited at the anodizing voltage of 320–360 V exhibited the uniformity and good corrosion protection properties after sealing with common agents.

Keywords Plasma electrolytic oxidation · Aluminum oxide · Carbon steel · Micro-arc anodizing

S. A. Karpushenkov · G. L. Shchukin · A. L. Belanovich · V. P. Savenko
Chemical Department, Belarusian State University, Leningradskaya Str. 14, 220050 Minsk, Belarus

A. I. Kulak (✉)
Institute of General and Inorganic Chemistry, National Academy of Sciences of Belarus, Surganova Str. 9, 220072 Minsk, Belarus
e-mail: kulak@igic.bas-net.by

1 Introduction

Anodizing of the valve metals, predominantly aluminum and its alloys, as well as Ti, Zr, Mg in aluminate, silicate, phosphate, fluoride, and tungstate aqueous solutions under very high voltage (up to 250–300 V) is a well-known method for the preparation of ceramic and ceramic-like oxide coatings possessing excellent thermal wear and corrosion resistance, together with good tribological, interfacial adhesion, dielectric, and heat insulation properties [1–12]. This method usually designed as plasma electrolytic oxidation, plasma-, microarc-, spark- or arc-anodizing is based on a combined action of electrochemical anodic oxidation, high-voltage spark, and local high-temperature treatment. It was successfully used in automotive industry as well as in the production of electrolytic capacitors, optically black coatings for space telescopes and solar collectors, biomedical devices, aerospace, and textile machine components [1–3].

Using plasma electrolytic oxidation for anodizing of non-valve metals such as carbon steel, iron, copper, nickel, and other practically important metals is, however, hampered by the fact that at the initial stage of the oxidation, the barrier layer essential for converting the process into spark regime is not formed on the metal surface. One of the possibilities for solving this problem is a microarc oxidation of steel substrate preliminary coated by arc spraying aluminum [13]. Besides, we have demonstrated the possibility for the formation of a barrier-like layer on the iron surface not by means of iron substrate oxidation but through the deposition of Al_2O_3 or SiO_2 layer resulted from the micro-arc decomposition of aluminate or silicate electrolyte [14, 15]. In the context of this approach, in this study we revealed the possibility for obtaining high-quality ceramic-like oxide coatings on iron surface by plasma

electrolytic anodizing in aqueous solutions of sodium aluminate.

2 Experimental

Plasma electrolytic anodizing of iron surface was conducted under voltstatic conditions using a DC power supply with voltage and current ranges of 0–400 V and 0–15 A, respectively. The power supply provided constant voltage with an accuracy of about ±4% of the desired value. The single-compartment two-electrode electrochemical cell contained 500 mL of electrolyte. The temperature of the electrolyte was kept within a range of 45–50 °C using cold water circulating through a heat exchanger. To reduce temperature and concentration gradients in the electrolyte, the solution was magnetically stirred. No more than 10 specimens were coated in a single freshly prepared electrolyte solution. Aqueous solution of 0.1 M $NaAlO_2$ + 0.05 M NaOH was prepared using commercial pure reagents and distilled water.

The working electrode (anode) was made from a grade of carbon steel with the surface area of 2 cm^2 and the composition in wt% 0.35 C, 0.8 Mn, <0.05 S, and <0.05 P. A plate of stainless steel EN 1.4301 (C 0.035%, Cr 18%, Ni 8.5%) was used as a cathode. The cathode area was approximately 20 times larger than that of the anode. Prior to anodizing, the electrodes were ground with emery paper and rinsed with organic solvents, surfactant-containing solution, and distilled water.

The corrosion resistance of oxide coatings was assessed from potentiodynamic polarization curves which were recorded using a PI-50-1 potentiostate in 0.5 M NaCl aqueous solution in a contact with air at room temperature in a conventional three-electrode electrochemical cell with a Pt counter-electrode and a saturated Ag | AgCl | KCl reference electrode (+0.201 V versus SHE); potential sweep rate was 2 mV s^{-1}.

The microhardness of the coatings was evaluated using a PMT-3 (Hv) microhardness tester with Vickers indenter at 50 g load. Thickness evaluation of the oxide coatings was performed by means of scanning electron microscopy on the polished cross-sections of the samples mounted in an epoxy resin. Several parallel measurements (typically 5–10) were performed in order to provide statistically significant data on the coating microhardness and thickness.

The X-ray diffraction (XRD) patterns were obtained using DRON-3.0 X-ray diffractometer at Co K_α radiation, MnO_2 filter, in $\theta/2\theta$ mode scans from 10° to 90° with a rate of 2°2θ min^{-1}.

The XPS measurements were performed with Perkin-Elmer 5400 ESCA X-ray spectrometer using Mg K_α X-ray beam (1,253.6 eV). The binding energy scale was calibrated with the E_b(Au $4f_{7/2}$) line at 84.0 eV. Elemental analysis of the coatings was carried out using PHI-660 Auger electron spectrometer.

Scanning electron microscopy (SEM) observation and electron probe microanalysis were performed with LEO-1455 VP microscope.

3 Results and discussion

It is visually seen that the application of the voltage higher than 200 V to the electrochemical cell results in a generation of small single spark discharges yellow in color. Further increase of the applied voltage leads to the enhancement of the sparking so that under $U \geq 250$ V one can observe an intense light emission being indicative of the change from conventional galvanic anodic oxidation to the micro-arc anodizing process. As this took place, marked changes in the time dependencies of anodic current (I, t) under pre-spark (Fig. 1a) and micro-arc (Fig. 1b) regimes are evident.

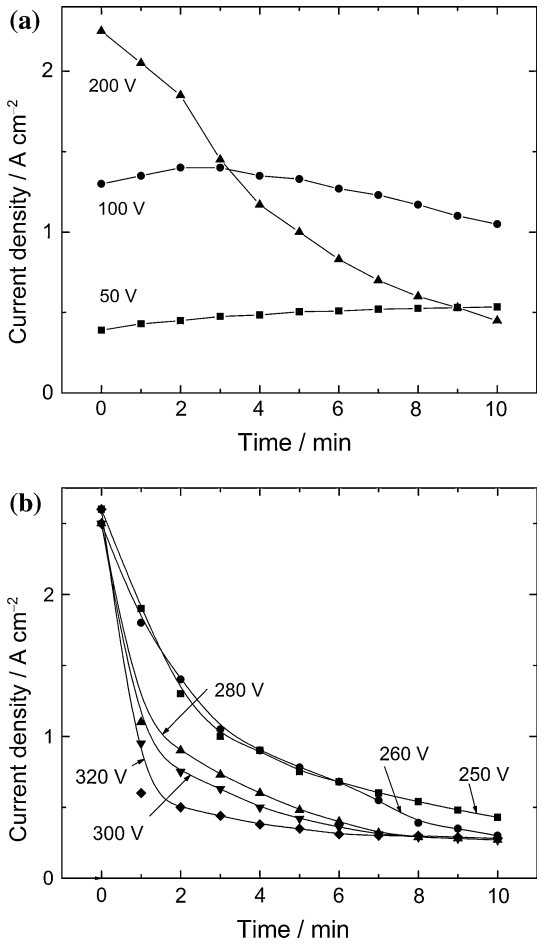

Fig. 1 Current–time dependencies for the anodizing processes in pre-spark (**a**) and micro-arc (**b**) ranges of voltages. Electrode (anode)—iron; electrolyte: 0.1 M $NaAlO_2$ + 0.05 M NaOH

At the micro-arc anodizing regime, the I, t curves are characterized by the decay of current from 2.5 to 0.5–0.7 A cm^{-2}, so that the higher is applied voltage, the more drastic is the current drop (Fig. 1b). Under high applied voltage ($U \geq 320$ V), within 4–5 min of the beginning of oxidation, the current value becomes almost invariable with time, and the oxide film growth proceeds as practically stationary process. As is apparent from the current density–voltage dependences (Fig. 2, curve 1) derived from the I, t curves for a fixed time interval equal to 1 min, the increase of the current at the voltage ranged from 50 to 200 V changes to its further decay which is due to the predominant passivating effect of the oxide coating formed in the range of 200–320 V. It is clearly seen that, at the micro-arc regime, the greater is the voltage, the less is the value to which the current drops within a fixed time interval.

In the case of 10 min fixed interval of anodizing (curve 2 in Fig. 2), which corresponds to a quasi-steady growth of aluminum oxide coating, the current declines immediately after exceeding voltage 100 V.

By integrating the I, t curves shown in Fig. 1, the values of the electric charge Q passed through the electrode system in a fixed time interval have been calculated (Fig. 3, curve 1). To draw this curve, we considered the charge passed through the system for the time interval equal to 10 min during which the process of coating deposition established quasi-stationary state.

As is obvious from the obtained Q, t curve, the growth of the voltage in the range from 50 to 100 V is accompanied by increasing charge passed through the system in 10 min, whereas further voltage increase (up to 320 V) leads to more than two-fold drop of the charge value. It is reasonable that the maximum of the electric charge at 100 V (Fig. 3, curve 1) corresponds to the maximal current at the 10 min fixed time interval on Fig. 2 (curve 2). Such a decrease of the charge may be associated with an enhanced passivating effect of the oxide coating due to the growth of the oxide coating thickness with increasing voltage (Fig. 4). It can be inferred that one of the reasons for obviously antibatic dependence of the coating thickness on the value of the passed charge at the micro-arc regime is an increase of the contribution of non-Faraday's processes with a rise in voltage. In particular, the contribution of the thermal component increases with increasing average power density ($P = QVt^{-1}$; P, V dependency is given in Fig. 3, curve 2).

It should be noted that the P values calculated by this means, while proportional to the thermal energy liberated

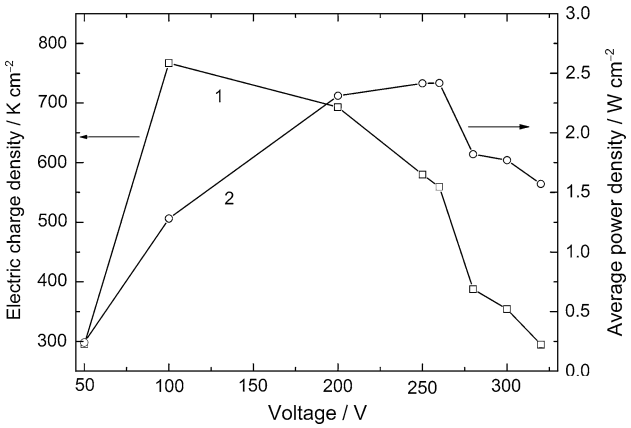

Fig. 3 Voltage dependencies of an electric charge density (*1*) and an average power density (*2*) after 10 min anodizing of iron electrode in aluminate electrolyte

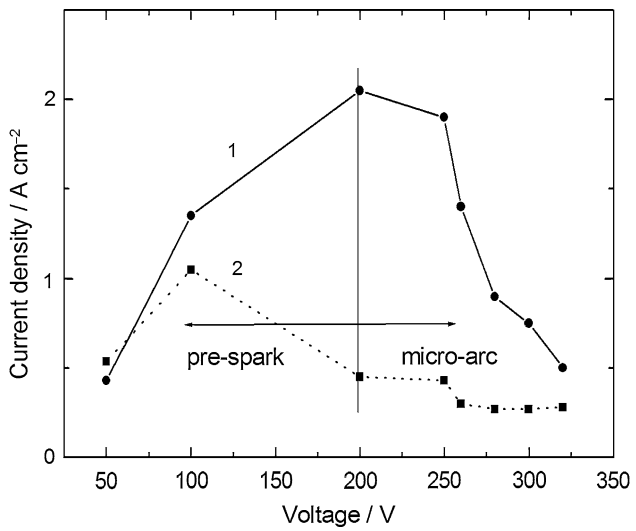

Fig. 2 Voltage dependency of the current density after 1 min (*1*) and 10 min (*2*) anodizing derived from the I, t curves presented in Fig. 1

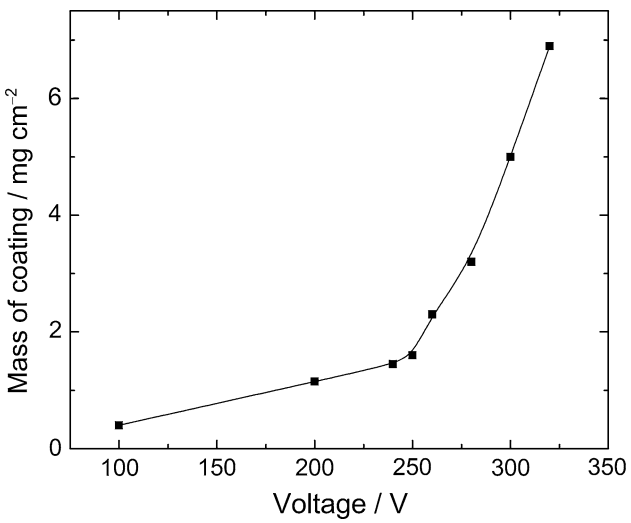

Fig. 4 Voltage dependency of the mass of deposited oxide in the process of iron anodizing in aluminate electrolyte during 10 min

at the anode, do not represent the absolute values of this energy since on such examination, we do not take into consideration a distribution of the voltage between different regions of the electrode system (at the near-electrode region, inside the passivating layer, in the volume of the electrolyte, and at the counter-electrode). From the comparison of curves 1 and 2 (Fig. 3), it is evident that the maximal electric charge is seen at 100 V that is in the pre-spark region, whereas the maximal power density is observed at 250–260 V that is in the range of micro-arc coating deposition.

It should be noted that there is no direct correlation between the rate of the coating deposition and the power expended. As is seen from Fig. 4, a sharp increase in the mass of deposited coatings is observed starting from 250 V and up to 320 V, even though the power density tends to diminish (Fig. 3, curve 2).

The lack of a straightforward correlation between the rates of the coating deposition and the values of both the electric charge and power density is probably due to a complicated combination of the electrochemical and thermal-stimulated processes

3.1 Electrochemical deposition

(a) Direct oxidation

$$\left[\mathrm{A1(OH)_4}\right]^- \rightarrow \left[\mathrm{A1(OH)_4}\right]^{\bullet} + \mathrm{e} \rightarrow \left[\mathrm{A1(OH)_3\,(OH)^{\bullet}}\right] \quad (1a)$$

$$2\left[\mathrm{A1(OH)_3(OH)^{\bullet}}\right] \rightarrow \left[2\mathrm{A1(OH)_3{\cdot}H_2O_2}\right] \rightarrow 2\mathrm{A1(OH)_3} + \mathrm{H_2O} + {}^1\!/_2\mathrm{O_2} \quad (1b)$$

$$\left[\mathrm{A1(OH)_4}\right]^- \rightarrow \mathrm{Al(OH)_3} + {}^1\!/_2\mathrm{O_2} + 2\mathrm{H_2O} + e \quad (2)$$

$$2\left[\mathrm{A1(OH)_4}\right]^- \rightarrow \mathrm{Al_2O_3} + {}^1\!/_2\mathrm{O_2} + 4\mathrm{H_2O} + 2e \quad (3)$$

(b) Indirect deposition

$$2\mathrm{OH^-} \rightarrow {}^1\!/_2\mathrm{O_2} + \mathrm{H_2O} + 2e \quad (4a)$$

$$\mathrm{H_2O} \rightarrow {}^1\!/_2\mathrm{O_2} + 2\mathrm{H^+} + 2e \quad (4b)$$

$$2\left[\mathrm{A1(OH)_4}\right]^- + 2\mathrm{H^+} \rightarrow 2\mathrm{Al(OH)_3} + 2\mathrm{H_2O} \rightarrow \mathrm{Al_2O_3} + 3\mathrm{H_2O} \quad (5)$$

(c) Thermal deposition

$$2\left[\mathrm{A1(OH)_4}\right]^- \rightarrow \mathrm{Al_2O_3} + 2\mathrm{OH^-} + 3\mathrm{H_2O} \quad (6)$$

$$\left[\mathrm{Al(OH)_4}\right]^- \rightarrow \mathrm{Al(OH)_3} + \mathrm{OH^-} \quad (7a)$$

$$2\mathrm{Al(OH)_3} \rightarrow \mathrm{Al_2O_3} + 3\mathrm{H_2O} \quad (7b)$$

(d) Anodic oxidation of iron substrate

$$\mathrm{Fe} + 3\mathrm{OH^-} \rightarrow \mathrm{Fe(OH)_3} + 3e \quad (8a)$$

$$\mathrm{Fe} + 3\mathrm{OH^-} \rightarrow \mathrm{FeOOH} + 3e + \mathrm{H_2O} \quad (8b)$$

$$2\mathrm{Fe} + 6\mathrm{OH^-} \rightarrow \mathrm{Fe_2O_3} + 6e + 3\mathrm{H_2O} \quad (8c)$$

Taking into account that the process of the coating deposition proceeds under high voltages in the electrolyte with a high electric conductivity, it is reasonable to assume that the electrode potential is many times higher than the overpotential of every above-listed electrode process (1)–(4), (8). All these processes involve the electrolyte components. Therefore, the contribution of each of them to the overall process of coating formation may strongly depend on the local concentrations of these components nearby the anode surface.

We suppose that the processes of direct oxidation of aluminate anion can be described with Eqs. 1–3 on the analogy of anodic oxidation of silicate anion under plasma electrolytic oxidation aluminum in silicate electrolyte [16]. Aluminum hydroxide precipitation (Eq. 5) from aluminate solutions under various pH and temperature is studied in details in [17–19].

It is hardly possible to determine the exact contributions of every above-listed process on a basis of experimental data we presently have. Since the concentration of water molecules (ca. 55 mol L^{-1}) is much higher than that of aluminate ions (0.1 mol L^{-1}), one might expect that an indirect deposition (4, 5) makes the greatest contribution to the overall process of coating deposition. It may be suggested that a sharp increase in the thickness of the deposited coating at the voltage higher than 250 V is mainly associated with the processes of indirect deposition (4a, 4b, 5), because in circumstances where the rate of generation of H^+ ions is high they have not managed to diffuse from the near-electrode region. This may lead to a significant local pH lowering in the vicinity of the anode which may cause the deposition of aluminum hydroxide and/or aluminum oxide. An important role of the processes of indirect deposition is circumstantially confirmed by the data [20–22] which indicates that the ratio (n) of OH^- to aluminum ion concentrations determines the character of the hydrolytic processes. For instance, in the range of stable solutions ($n = 4.4$, pH > 13.0), the monomer aluminate ions prevail; at $n = 3.3$–4.4 and pH 9.3–12.8 the polymers with the composition $[Al(OH)_4]_n(OH)_2^{(n+2)-}$ are being

formed; in the range where $n = 3.01–3.3$, pH 8.2–9.3 one can observe a rapid generation of the mixture of colloid $Al(OH)_3$ and polymeric $[Al(OH)_4]_n(OH)_2^{(n+2)-}$ and $[Al(OH)_3]_n(OH)_2^-$, the latter constituting also the colloid particles. A similar transformation of the monomer aluminate ions to the polymer aluminates followed by their precipitation would thus be expected under the conditions of plasma electrolytic anodizing where pH sharply drops and temperature arises in the near-electrode region.

Under these conditions, an additional generation of aluminum oxide or hydroxide could be possible as a result of a direct anodic oxidation of aluminate anions in accordance with (1–3) reactions. In this case, a removal of hydroxyl group from an aluminate anion is a result of its oxidation, similarly to the oxidation of hydroxyl group in an electrolyte (4a).

The contribution of the thermal decomposition of aluminate anions essentially depends on the pH value in near-electrode region because, as is well-known, this process is reversible and amorphous aluminum hydroxide could dissolve with a generation of aluminate ions [20].

An admixture of iron is maximal in the case of pre-spark regime; it results from anodic oxidation of iron substrate and the formation of iron oxides/hydroxides mixture [23]. A generation of soluble iron species such as ferrate ions is unlikely because the concentration of the alkali is not sufficient for this process [24].

As a result of all these processes combined, we obtain the coatings with a distinctive porous surface (Fig. 5) similar in appearance to that of aluminum oxide films prepared by the plasma electrolytic anodizing of aluminum. The coating obtained in spark regime at 320 V possesses a flowed crater-like structure with reach-through conic pores having an outer diameter up to 5 μm (Fig. 5b).

The thickness of such coatings estimated from their SEM images increases with increasing time of anodizing from 0.3–0.5 μm at 1 min and 2.5–4 μm at 10 min to 25–30 μm at 1 h; however, these values should be regarded merely as a result of a rough assessment since the films are strongly irregular in thickness.

A microprobe elemental analysis of these coatings (Fig. 6) has revealed that they contain admixed iron along with aluminum. Since a generation of iron ions in the coatings is a result of iron substrate oxidation (reactions 8a–8c) followed by the diffusion of ions through the pores in aluminum oxide film, the concentration of iron decreases with increasing film thickness, and it is maximal at the bottom of the pores. Hence the coatings formed in pre-spark regime are enriched with iron. For instance, the coatings deposited at 100 V are composed of iron hydroxide/oxide admixed with 18 at. % alumina, the films prepared at 200 V consist of oxide mixture with an average ratio Fe:Al = 1:1.84, and those obtained at 300 V are

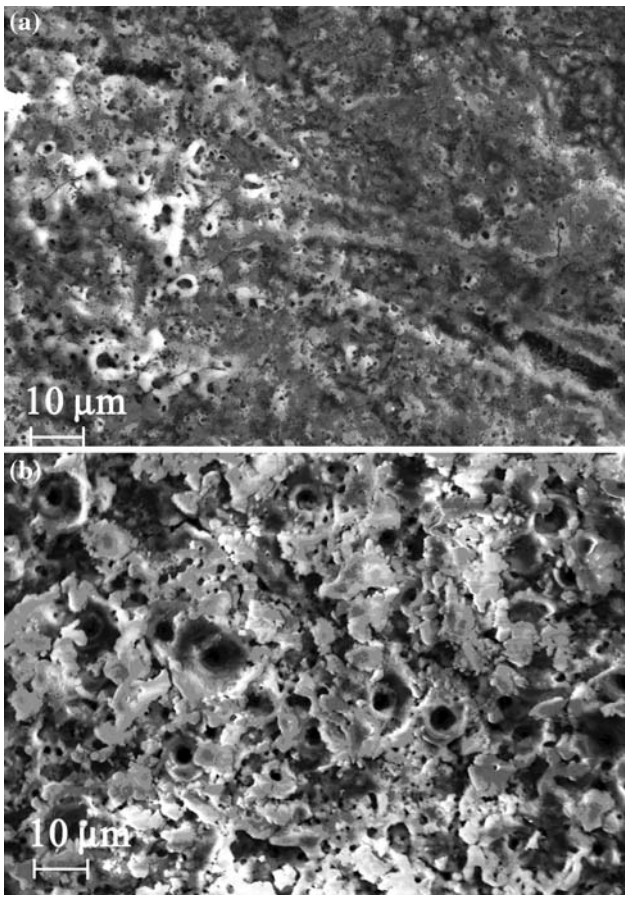

Fig. 5 Typical SEM images of the coatings deposited onto iron substrates during 10 min in micro-arc regime at 200 V (**a**) and 320 V (**b**)

aluminum oxide admixed with only 5 at. % iron oxide. Accordingly, the color of the coatings changes from intense beige in the case of the films obtained in pre-spark regime (100–200 V) to light gray for the samples prepared at 300 V and grayish white for those deposited at 320 V.

Elemental analysis of the deposited films by Auger spectroscopy confirms the presence of impure iron in aluminum oxide coatings. The atomic concentration of iron calculated in terms of sensitivity factors may amount to as much as 17.7% and, in the case of the coatings obtained by a long-time deposition (>30 min) at high voltages (>300 V), the ratio of aluminum-to-oxygen atomic concentrations is close to Al:O = 2:3.

The distinctions between the values of iron concentration determined by Auger and electron probe microanalysis may stem from the differences in a deepness of the surface layers which are probed by the above methods. In other words, the difference in the values obtained by both techniques may be attributed to the fact that the enrichment of the coatings with iron takes place predominantly in the layers closest to the iron support and diminishes with

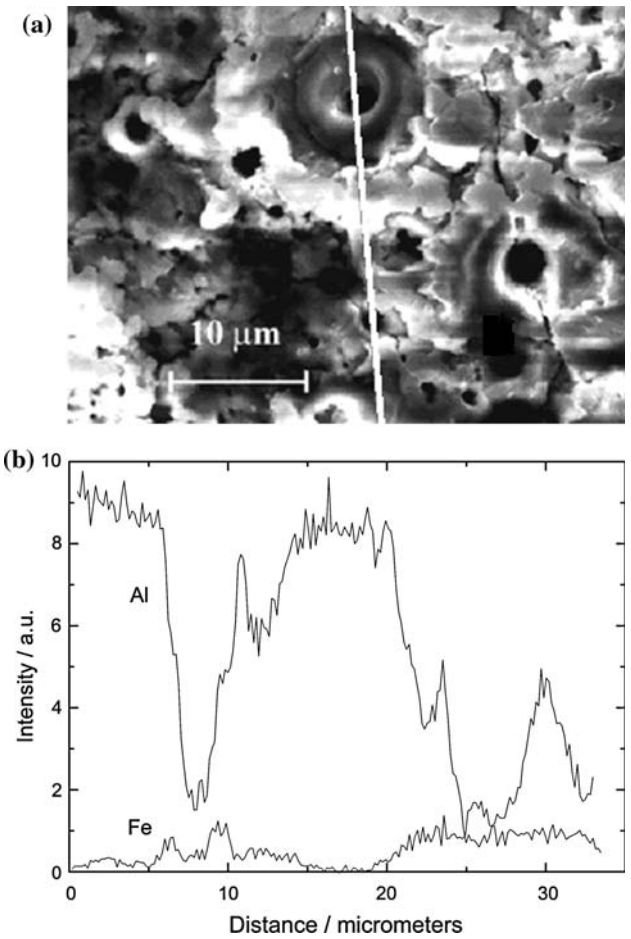

Fig. 6 Typical SEM image of crater-like-porous surface (**a**) and the coordinate distribution of the main elements (**b**) for the micro-arc deposited (320 V, 30 min) aluminum oxide coating on a iron substrate

distance from it. Both the inner surface and the bottoms of the pores, which are enriched with iron, contribute additionally to the results of these measurements (Fig. 6).

According to the data of XPS analysis, the near-surface layer of the coatings (no more than 10 nm in thickness) contains, along with main elements such as Al, O, and C, only trace amounts of Fe. In the case of relatively thin coating obtained by 1 min anodizing, the $E_{O\ 1s}$ core-level peak is located at 531.4 eV (Fig. 7a) that is in agreement with the value determined for the polycrystalline Al_2O_3 [25–28].

In the case of thicker coating formed by 30 min anodizing, the binding energy is slightly lowered, and the $E_{O\ 1s}$ core-level peak is located at 530.2 eV that is also close to the literature data for Al_2O_3 [25–28]. It should be noted that in some papers the $E_{O\ 1s}$ value equal to 531.4 eV has been given for hydrated aluminum oxide ($Al_2O_3 \times 3H_2O$, gibbsite) and about 531.1 eV—for the hydroxide $Al(OH)_3$ [29, 30]. Hence it is impossible to separate the contributions of aluminum oxide and hydroxide only on the basis of $E_{O\ 1s}$ value.

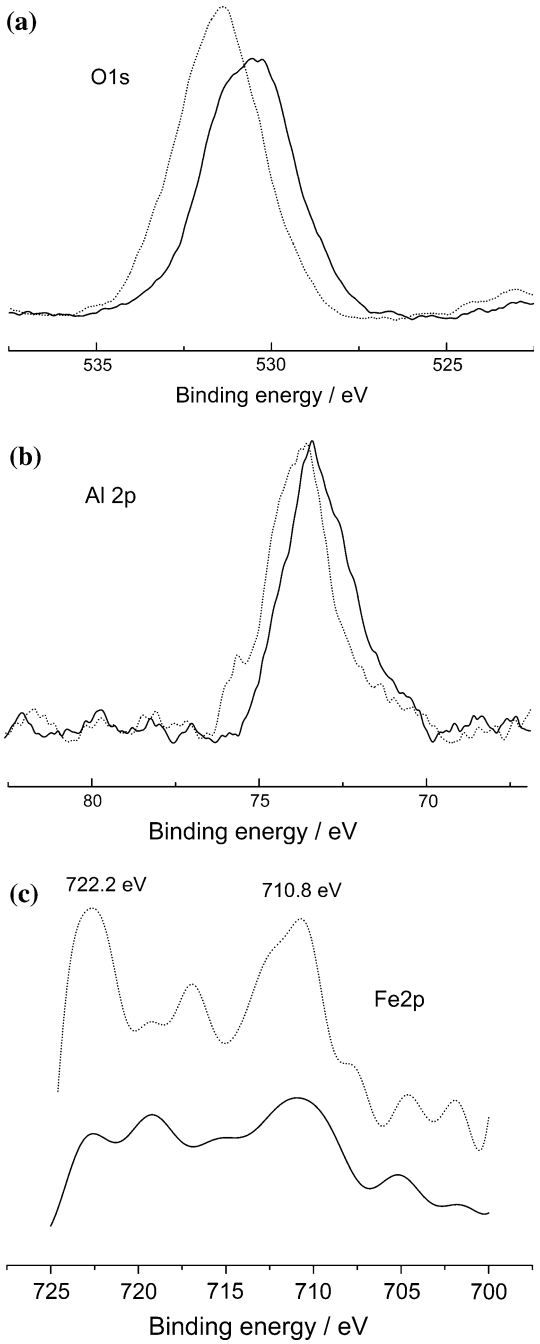

Fig. 7 XPS O 1s (**a**), Al 2p (**b**) and Fe 2p (**c**) core-level spectra of the coatings micro-arc deposited onto iron substrate at 320 V in aluminate electrolyte during 1 min (*dotted line*) and 10 min (*solid line*)

Similar problems emerge when we attempt to identify the content of the coatings relaying on the location of the $E_{Al\ 2p}$ core-level peak. For every coating obtained in this work, the $E_{Al\ 2p}$ value determined from the XPS spectrum (Fig. 7b) is approximately the same (73.7–74.3 eV) coinciding with that given previously for Al_2O_3 [26–28, 31]. On the other hand, a very close $E_{Al\ 2p}$ value (74.4 eV) has

been inferred for the hydrated aluminum oxide (gibbsite) [27], 73.9–74.3 eV for boehmite and pseudoboehmite AlO(OH) [27, 28].

XPS spectrum of a relatively thin coating prepared at 1 min anodizing exhibits additional peaks at 710.8 and 722.6 eV attributed to Fe $2p^{3/2}$ and Fe $2p^{1/2}$,correspondingly (Fig. 7c). According to the literature data, the peaks corresponding to a binding energy of 710.8 ± 0.2 and 711.4 ± 0.2 eV are characteristics for the Fe $-2p^{3/2}$ of Fe_2O_3 and FeOOH, respectively [32]. Contrary to this, in the other work [33], it was reported that the 2p spectra of Fe_2O_3 and FeOOH were practically identical. Thus, using the XPS spectrum we can only conclude that iron is in Fe(III) form, probably as oxide–hydroxide inclusions. Due to a very low surface concentration of iron in thick coatings it is not detected on their XPS spectra (Fig. 7c).

In addition to the XPS data which characterized a very thin (up to 10 nm) surface layer, we have registered FTIR reflectance and XRD spectra that provided a mean for analyzing the properties of a deeper part of the coatings. As is seen from the FTIR spectra (Fig. 8), with an increase in anodizing time and, correspondingly, the formation of thicker coatings, one can observe an essential decrease in the absorbance at 1,057–1,065 cm^{-1} characteristic for the δ_{AlOH} vibrations Al–OH in boehmite γ-AlOOH [34], as well as the bands at 690 and 770 cm^{-1} characteristic of both thin and thick coatings are probably attributed to the OH-translation vibrations in boehmite [34]. The band at 970–980 cm^{-1} could be assigned to Al–OH deformation in dawsonite-like component of the coating [35].

Taking into account that the surface of the thinnest coatings are enriched with iron, the shoulder at 879 cm^{-1} in the spectra of such films may be due to the vibrations of Fe–OH bonds; however, in this region the bands attributed to the vibrations of Al–O bonds in Al_2O_3 can also appear. In this spectral region (below 1,000 cm^{-1}), Al–O–Al stretching and bending vibrations are unsplit and broad because of the poor degree of the oxide–hydroxide coating crystallinity. The latter vibrations may be responsible for the appearance of the bands at 479 and 976 cm^{-1} in the spectra of the thick films.

In high-frequency spectral region, the wide band originated from the O–H stretching vibrations of absorbed water molecules are seen at 3,000–3,600 cm^{-1}. Accordingly, the absorption at 1,634 cm^{-1} in the spectra of thick films can be attributed to the bending vibrations of water molecules. The absorption in the range of 1,400–1,600 cm^{-1} may be connected with the formation of various carbonate complexes and surface species which have a dawsonite-like structure. The latter can be formed as a result of the interaction between Na^+ ions, dissolved CO_2, and water [36]. On the whole, the data of FTIR spectroscopy testify that on the initial stages of deposition (at the time of anodizing equal to 1–5 min), the deposited films contain Al_2O_3 along with γ-AlO(OH) and, probably, aluminum hydroxide, while the thick coatings obtained by the deposition for 30–60 min can be enriched with of aluminum oxide.

The X-ray diffraction analysis shows that the main oxide–hydroxide components of the obtained coatings [AlO(OH), $Al(OH)_3$, Al_2O_3] are predominantly amorphous, and well-defined diffraction patterns characteristic of the crystalline corundum are observed only for the thick coatings deposited during 10–60 min (Fig. 9). The data of XRD analysis testify that the content of crystalline corundum (α-Al_2O_3) phase

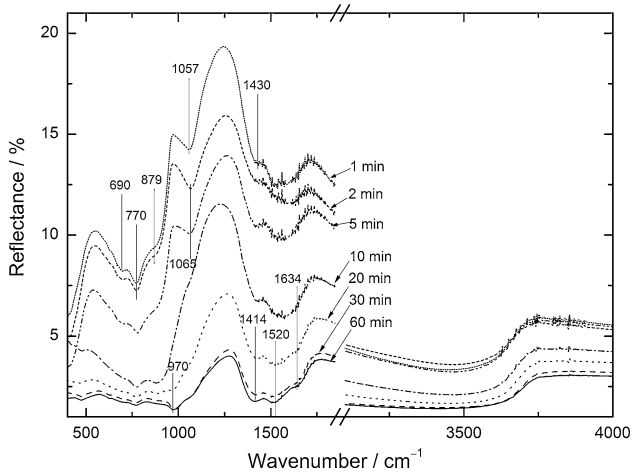

Fig. 8 FTIR reflectance spectra of the coatings deposited onto iron substrate during different intervals of micro-arc anodizing in aluminate electrolyte at 320 V

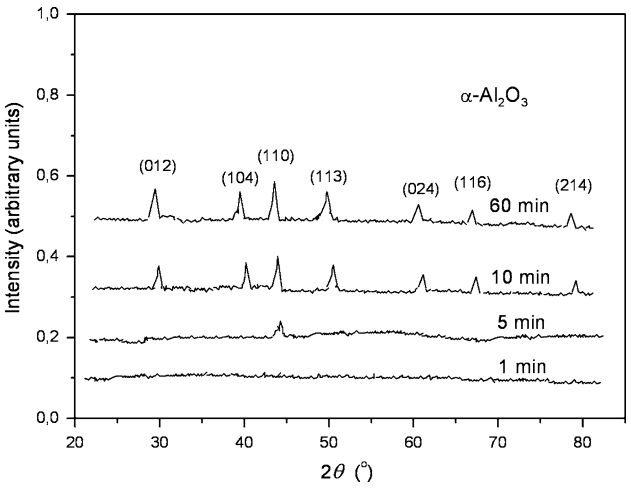

Fig. 9 XRD patterns of the aluminum oxide coatings prepared by micro-arc deposition at 320 V in aluminate electrolyte for various deposition intervals

increases with an increase in anodizing time, i.e., with a growth of coating thickness (Fig. 9). Probably, an enrichment of the coatings with corundum is responsible for the essentially enhanced micro-hardness of the iron coated with aluminum oxide (the micro-hardness of the coatings deposited for 30 min at 320 V is equal to 2 GPa, while that of untreated iron substrate is 0.68 GPa).

It should be noted that, in spite of their porosity, the coatings deposited at micro-arc conditions ensure some corrosion protection. As is seen from the potentiodynamic polarization curves (Fig. 10a) obtained in sodium chloride test solution, the deposited aluminum oxide coatings affect predominantly the cathodic part of polarization curves. The increase of this effect with growing thickness of the oxide coating can be attributed to the enhancement of diffusion limitations during the cathodic reduction of oxygen. Increasing the duration of anodizing process from 1 to 5–10 min leads to a similar result (Fig. 10b). Some deterioration of protective properties of the coatings obtained under prolonged anodizing (about 60 min) can be associated with enhancing formation of the cracks and increasing number of through pores provided access for the electrolyte to the surface of iron support. The values of corrosion exchange current (i_{corr}) calculated from the intersection of the linearized cathodic and anodic parts of polarization curves and the values of corrosion potentials are given in Table 1. It should be noted that a decrease in corrosion currents caused by the micro-arc deposition of aluminum oxide films is limited by a high porosity of these letter, so that they obviously cannot be regarded as efficient protective coatings.

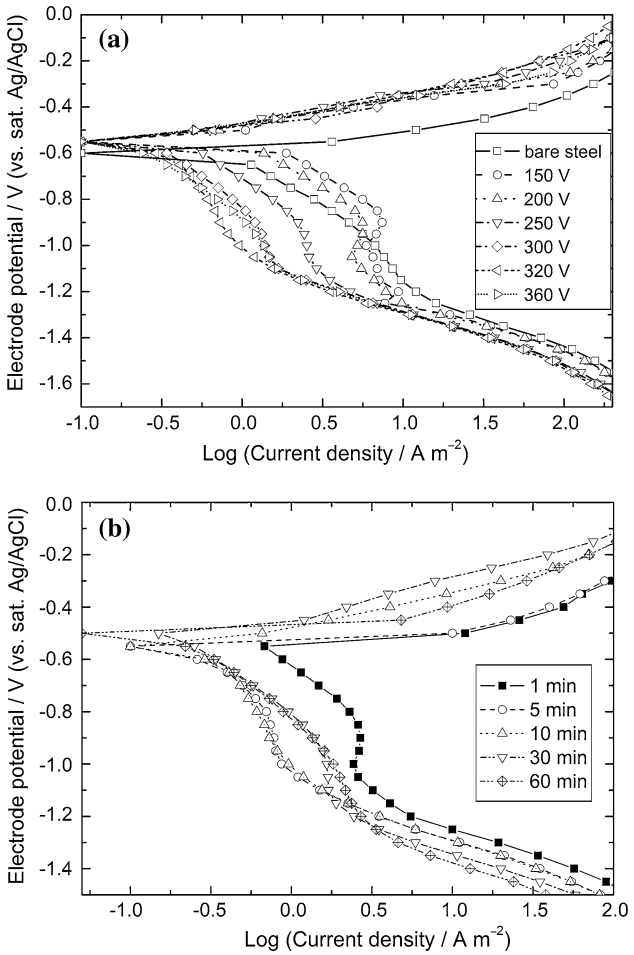

Fig. 10 Potentiodynamic current–potential curves for the iron electrodes covered with aluminum oxide coatings deposited under various voltages and constant time equal to 10 min (**a**); under various operating time and constant voltage equal to 320 V (**b**). Potential sweep rate: 2 mV s^{-1}. Electrolyte: aqueous 0.5 M NaCl solution

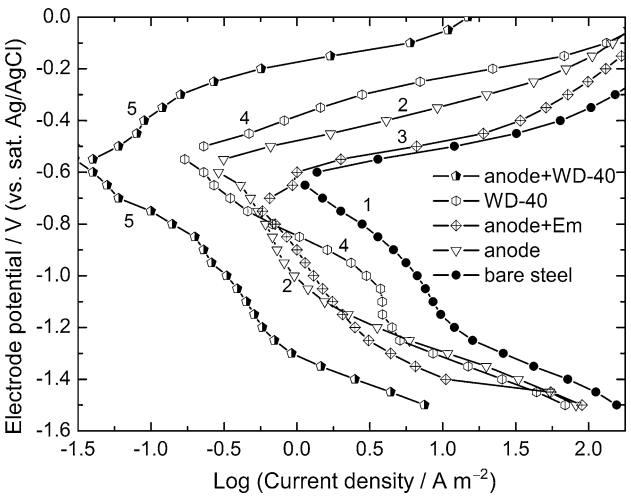

Fig. 11 Potentiodynamic current–potential curves for bare iron electrode (*1*), iron covered with aluminum oxide coating deposited at 320 V during 10 min, as-deposited (*2*), and after additional coating with silicon emulsion (*3*) or WD-40 (*5*); iron electrode treated with WD-40 without aluminum oxide interlayer (*4*). Potential sweep rate: 2 mV s^{-1}. Electrolyte: aqueous 0.5 M NaCl solution

Table 1 Corrosion potential (versus sat. Ag/AgCl) and corrosion current density values in 0.5 M NaCl aqueous solution for bare iron electrode and for aluminum oxide-coated samples prepared by anodizing iron substrates in aqueous 0.1 M $NaAlO_2$ + 0.05 M NaOH at 320 V for 10 min

Anodizing voltage, V	Bare steel	150	200	250	300	320	360
Corrosion potential, V	−0.58 ± 0.02	−0.48 ± 0.01	−0.48 ± 0.01	−0.53 ± 0.01	−0.52 ± 0.01	−0.54 ± 0.01	−0.54 ± 0.01
Corrosion current density, A m^{-2}	0.86 ± 0.11	0.95 ± 0.07	0.78 ± 0.06	0.40 ± 0.03	0.34 ± 0.02	0.32 ± 0.02	0.19 ± 0.01

Table 2 Corrosion potential (versus sat. Ag/AgCl) and corrosion current density values in 0.5 M NaCl aqueous solution for aluminum oxide-coated samples prepared by anodizing iron substrates in aqueous 0.1 M $NaAlO_2$ + 0.05 M NaOH at 320 V for 10 min, as anodized and after sealing with WD-40 or silicon emulsion

Treatment	Anodizing at 320 V	WD-40	Anodizing + silicon emulsion	Anodizing + WD-40
Corrosion potential, V	−0.54 ± 0.01	−0.55 ± 0.02	−0.62 ± 0.01	−0.51 ± 0.07
Corrosion current density, A m^{-2}	0.32 ± 0.02	0.13 ± 0.01	0.42 ± 0.02	0.03 ± 0.01

On the other hand, the porous structure of the coatings provides the possibility for improving their protective properties by way of impregnation with sealing agents. We have investigated the potentialities of this approach using common sealing agents such as Silicone Resin Emulsion SILRES® BS 1001 (water-thinnable solventless emulsion based on a mixture of silane and siloxane) produced by Wacker-Chemie AG, and a commercial product WD-40 based on the oil and corrosion inhibitor and lubricant, manufactured by WD-40 Company, USA .

As is seen from the potentiodynamic polarization curves (Fig. 11), sealing the aluminum oxide coatings with silane–siloxane emulsion does not lead to significant improvements in corrosion protection, whereas sealing with the oil WD-40 causes a substantial decrease in corrosion currents (Table 2). It should be noted that a mere application of WD-40 oil on a bare surface of iron substrate does not work well; the protective action of such obtained coating is brief, and under aqueous conditions, it disappears in several hours.

Hence, the most pronounced corrosion protection effect results from sealing the micro-arc anodized iron with WD-40 oil. This treatment allows reducing corrosion current density by a factor of 30 in comparison with that for the bare iron substrate. It should be noted that this result should not be regarded as maximally achievable; it only illustrates the principal possibility for using the micro-arc-fabricated aluminum oxide film as an adhesive underlayer for the preparation of corrosion-protective coatings on iron substrate.

4 Conclusions

To summarize, we have demonstrated the possibility for the use of plasma electrolytic anodizing technique for the preparation of aluminum oxide films on the surface of a non-valve metal such as iron. For this purpose, we have used the aluminate electrolyte decomposed at the electrode surface with the result that the aluminum oxide film is formed which on the initial stages of this process acts as a barrier layer favorable for changing the anodizing process to the micro-arc regime. From the data of XRD, FTIR, and Auger spectroscopy, it has been established that in micro-arc regime at the voltage of 240–360 V, it is possible to prepare the porous ceramic-like coatings with a thickness up to tens of micrometers consisting of aluminum oxide-included corundum phase (α-Al_2O_3). The films with a thickness of 4–15 μm obtained under anodizing at 320–360 V during ca. 10 min exhibited the best combination of the uniformity and mechanical properties. Corrosion protection properties of these coatings could be easily improved using a common sealing procedure.

The coatings such obtained are prominent for the deposition onto the surface of iron in order to manage its surface properties, to enhance chemical and corrosion stability, and possibly to create novel composite coatings through further filling of the pores with the particles of catalysts, photocatalysts, pigments, as well as biocompatible and other functional components.

References

1. Yerokhin AL, Nie X, Leyland A, Matthews A, Dowey SJ (1999) Surf Coat Technol 122:73
2. Kuhn AT (2002) Met Finish 100:44
3. Matykina E, Monfort F, Berkani A, Skeldon P, Thompson GE, Gough J (2007) J Electrochem Soc 154:C279
4. Blawert C, Heitmann V, Dietzel W, Nykyforchyn HM, Klapkiv MD (2005) Surf Coat Technol 200:68
5. Arrabal R, Matykina E, Skeldon P, Thompson GE, Pardo A (2008) J Electrochem Soc 155:C101
6. Habazaki H, Onodera T, Fushimi K, Konno H, Toyotake K (2007) Surf Coat Technol 201:8730
7. Gnedenkov SV, Khrisanfova OA, Zavidnaya AG, Sinebrukhov SL, Kovryanov AN, Scorobogatova TM, Gordienko PS (2000) Surf Coat Technol 123:24
8. Gnedenkov SV, Khrisanfova OA, Zavidnaya AG, Sinebrukhov SL, Gordienko PS, Iwatsubo S, Matsui A (2001) Surf Coat Technol 145:146
9. Klapkiv M, Povstyana N, Nykyforchyn H (2006) Mater Sci 42:277
10. Nykyforchyn HN, Agarwala VS, Klapkiv MD, Posuvailo VM (2008) Adv Mater Res 38:27
11. Curran JA, Clyne TW (2005) Surf Coat Technol 199:177
12. Voevodin AA, Yerokhin AL, Lyubimov VV, Donley MS, Zabinski JS (1996) Surf Coat Technol 86–87:516
13. Gu W, Shen D, Wang Y, Chen G, Feng W, Zhang G, Fan S, Liu C, Yang S (2006) Appl Surf Sci 252:2927
14. Karpushenkov SA, Shchukin GL, Belanovich AL, Savenko VP, Sviridov DV (2004) Proc Natl Acad Sci Belarus, Ser Chem 3:57
15. Shchukin GL, Belanovich AL, Karpushenkov SA, Savenko VP, Kolyago AE (2002) Proc Natl Acad Sci Belarus, Ser Chem 4:5

16. Belevantsev VI, Terleeva OP, Markov GA, Shulepko EK, Slonova AI, Utkin VV (1998) Protect Met 34:416
17. Van Straten HA, Holtkamp BTW, Bruyn PL (1984) J Colloid Interface Sci 98:342
18. Van Straten HA, Bruyn PL (1984) J Colloid Interface Sci 102:260
19. Panias D, Krestou A (2007) Powder Technol 175:163
20. Eremin NI, Volokhov YA, Mironov VE (1974) Russ Chem Rev 43:92
21. Chaplygina NM, Itkina LS, Petrova EV (1974) Russ J Inorg Chem 19:762
22. Panasko GA, Yashunin PV (1964) Russ J Appl Chem 37:285
23. Haupt S, Strehblow H-H (1987) Langmuir 3:873
24. Burleigh TD, Dotson TC, Dotson KT, Gabay SJ, Sloan TB, Ferrell SG (2007) J Electrochem Soc 154:C579
25. Paparazzo E (1986) Appl Surf Sci 25:1
26. Tian J, Luo Z, Qi S, Sun X (2002) Surf Coat Technol 154:1
27. Kloprogge JT, Duong LV, Wood BJ, Frost RL (2006) J Colloid Interface Sci 296:572
28. van den Brand J, Snijders PS, Sloof WG, Terryn H, de Wit JHW (2004) J Phys Chem B 108:6017
29. Sugama T, Kukacka LE, Carciello N, Hocker N (1989) Cem Concr Res 19:857
30. Wagner CD, Passoja DE, Hillery HF, Kinisky TG, Six HA, Jansen WT, Taylor JA (1982) J Vac Sci Technol 21:933
31. Wei T, Yan F, Tian J (2005) J Alloys Comp 389:169
32. Grosvenor AP, Kobe BA, Biesinger MC, McIntyre NS (2004) Surf Interface Anal 36:1564
33. Asami K, Hashimoto K (1978) In: Frankenthal RP, Kruger J (ed) Passivity metals. Electrochem. Soc. Inc., New Jersey, p 585
34. Geiculescu AC, Strange TF (2003) Thin Solid Films 426:160
35. Stoica G, Groen JC, Abello S, Manchanda R, Perez-Ramırez J (2008) Chem Mater 20:3973
36. Lee DH, Condrate RA Sr (1995) Mater Lett 23:241